Mechanistic differences between methanol and dimethyl ether in zeolite-catalyzed hydrocarbon synthesis

Felix M. Kirchberger[a,1], Yue Liu[a,1], Philipp N. Plessow[b], Markus Tonigold[c], Felix Studt[b,d], Maricruz Sanchez-Sanchez[a,2], and Johannes A. Lercher[a,2]

[a]Department of Chemistry and Catalysis Research Center, Technische Universität München, 85747 Garching, Germany; [b]Institute of Catalysis Research and Technology, Karlsruhe Institute of Technology, 76344 Eggenstein-Leopoldshafen, Germany; [c]Clariant Produkte (Deutschland) GmbH, 83052 Bruckmühl, Germany; and [d]Institute for Chemical Technology and Polymer Chemistry, Karlsruhe Institute of Technology, 76131 Karlsruhe, Germany

Water influences critically the kinetics of the autocatalytic conversion of methanol to hydrocarbons in acid zeolites. At very low conversions but otherwise typical reaction conditions, the initiation of the reaction is delayed in presence of H_2O. In absence of hydrocarbons, the main reactions are the methanol and dimethyl ether (DME) interconversion and the formation of a C_1 reactive mixture—which in turn initiates the formation of first hydrocarbons in the zeolite pores. We conclude that the dominant reactions for the formation of a reactive C_1 pool at this stage involve hydrogen transfer from both MeOH and DME to surface methoxy groups, leading to methane and formaldehyde in a 1:1 stoichiometry. While formaldehyde reacts further to other C_1 intermediates and initiates the formation of first C–C bonds, CH_4 is not reacting. The hydride transfer to methoxy groups is the rate-determining step in the initiation of the conversion of methanol and DME to hydrocarbons. Thus, CH_4 formation rates at very low conversions, i.e., in the initiation stage before autocatalysis starts, are used to gauge the formation rates of first hydrocarbons. Kinetics, in good agreement with theoretical calculations, show surprisingly that hydrogen transfer from DME to methoxy species is 10 times faster than hydrogen transfer from methanol. This difference in reactivity causes the observed faster formation of hydrocarbons in dry feeds, when the concentration of methanol is lower than in presence of water. Importantly, the kinetic analysis of CH_4 formation rates provides a unique quantitative parameter to characterize the activity of catalysts in the methanol-to-hydrocarbon process.

methanol to hydrocarbons | H-ZSM-5 | formaldehyde | hydrogen transfer

The catalytic conversion of methanol (MeOH) to hydrocarbons (MTH) and its variants to lower olefins (MTO), gasoline (MTG), or aromatic compounds (MTA) has evolved as the major route to produce hydrocarbons via a synthesis gas (1–4). For light alkene synthesis two types of molecular sieve catalysts, the aluminosilicate MFI and the silicoaluminophosphate of CHA, SAPO-34, have been commercialized and provide routes to propene and ethene, respectively. On first sight, the differences in selectivities between two groups of catalysts are mainly related to differences in the pore structures. However, the MTH reaction is a complex autocatalytic reaction with a dual-cycle mechanism involving multiple organic intermediates that can be regarded as cocatalysts (5). Zeolite porosity is only one of the parameters that affect the nature and mobility of the hydrocarbons entrained in the pores, and therefore the interplay of reaction conditions and stabilization and transport of reaction intermediates plays an important role in the final catalyst lifetime and product distribution that can be achieved.

It is a characteristic of the MTO process that the feedstock contacts the catalysts as a mixture of MeOH, dimethyl ether (DME), and water, in ratios determined by the acid-catalyzed reversible dehydration of MeOH. Even when only DME is used,

its conversion to hydrocarbons forms water. Using water to dilute hydrocarbons and to promote heat transfer has evolved as common practice in industrial applications, modulating inevitably the interconversion between MeOH and DME. Therefore, the differences in the reactivity between MeOH and DME to both alkenes as well as alkanes and aromatic molecules have been frequently addressed (6–11). The different reactivities of MeOH and DME would be less important if they were equilibrated under reaction conditions. However, reports show unequivocally that partial pressures of MeOH, DME, and water often deviate from equilibrium during MTO catalysis (9, 10).

The conversion of MeOH/DME on zeolites proceeds via several stages (12): 1) an initiation stage, during which the conversion is very low, but the first C–C bonds are formed and the resulting species are gradually converted to a hydrocarbon pool; 2) as soon as a certain concentration of hydrocarbons in the pores is reached (the hydrocarbon pool), methylation begins to dominate and MeOH and DME are rapidly and autocatalytically converted in a dual-cycle mechanism (13, 14);

Significance

Methanol conversion to hydrocarbons has emerged as a key reaction for synthetic energy carriers and light alkenes. The autocatalytic nature and complex reaction network make a mechanistic understanding very challenging and widely debated. Water is not only part of the overall conversion, it is also frequently used as diluent, influencing, in turn, activity, selectivity, and stability of the catalysts. Water directly and indirectly influences the processes that initiate the C–C formation via adjusting the chemical potential of methanol and dimethyl ether, with the latter being more efficient to generate highly reactive C_1 species via hydride transfer. The insight shows paths to optimize the stability of catalysts and to tailor the product distribution for H-ZSM-5–based catalysts.

[1]F.M.K. and Y.L. contributed equally to this work.

[2]To whom correspondence may be addressed. Email: m.sanchez@tum.de or johannes.lercher@ch.tum.de.

and 3) after complete conversion of methanol and DME, the interconversions between hydrocarbons, mainly light alkenes, alkanes, and aromatics, determine the final product distribution. In a fixed-bed reactor, this zoning leads to the characteristic S-shaped increase of the conversion with contact time, as illustrated in Fig. 1.

Understanding the impact of the feed composition (i.e., the relative concentration of MeOH, DME, and H_2O) on catalyst lifetime and activity is of fundamental importance to control activity, selectivity, and stability in industrial applications. DME has been reported to be more reactive than MeOH (9, 15). On the other hand, MeOH is generally regarded as more reactive for the reaction paths leading to nonalkene by-products and deactivation (9, 10, 16). Despite these reports, consensus has not been reached on the mechanistic origin of the reactivity differences observed between DME and MeOH. In practice, MeOH, DME, and water always coexist and their partial pressures change as a result not only of methylation reactions but also of the MeOH/DME interconversion. Therefore, a quantitative evaluation of the influence of a single component in the MTO mechanism requires complex experimental strategies. The highly reactive key mechanistic intermediates in the reaction pathways leading to nonalkene by-products and catalyst deactivation add additional challenges (17–19).

The observed effects of water on the overall turnover number capacity of MTH catalysts are compounded with the influence of a set of parameters including temperature, contact time, surface coverage, and acidity and pore size on the rates of autocatalytic reactions and deactivating reactions. In order to obtain the relevant kinetic parameters in the complex MTH reaction network it is necessary to perform measurements at conditions at which these opposing processes are decoupled.

Here, we report a kinetic study at selected MTO reaction conditions during which quasi-equilibration of DME, MeOH, and H_2O has been reached. Our experimental study was performed at very low conversions, to ensure that hydrocarbon chemistry and in particular fast methylation reactions are negligible. This allowed us to evaluate quantitatively the reactivity of DME and MeOH in the reaction steps that lead to the initiation of the hydrocarbon pool and the dual cycle. At the typical temperatures used in MTH and also in this work, the fast MeOH-to-DME interconversion takes place mediated by methoxy species (20). The formation of HCHO and equivalent intermediates such as CO is widely accepted as key step in the formation of the first C–C bond-containing products and

intermediates (18, 21–23). We provide quantitative evidence of a higher reactivity of DME for the formation of CH_4 and HCHO compared to MeOH, and, in good agreement, higher overall rates for the autocatalytic MTH conversion in the absence of water. Our results also demonstrate that methylation rates in the production of olefins by the dual-cycle mechanism mainly depend on the population of methoxy species and, thus, they are negatively affected by increasing concentrations of H_2O.

Properties of H-ZSM-5 Catalyst Used for the Mechanistic Study

It is known that a low concentration of Brønsted acid sites (BAS) minimizes the probability of a molecule to undergo successive reactions along the diffusion path leading to aromatization and coking (24). Therefore, in order to ensure viable reaction conditions at which the catalyst can operate within the initiation stage (I in Fig. 1), we have chosen to perform our experiments on steamed H-ZSM-5 with an Si/Al ratio of 90, a commercial methanol-to-propene catalyst provided by Clariant AG. The catalyst has 68 ± 4 $\mu mol \cdot g^{-1}$ BAS and 37 ± 2 $\mu mol \cdot g^{-1}$ Lewis acid sites, determined by adsorption of pyridine. The zeolite sample had 0.14 cm^3/g micropore volume, determined by N_2 adsorption.

MeOH and DME Interconversion

The acid-catalyzed reversible intermolecular dehydration of MeOH to DME is a primary reaction in MTH. Here, as we start from mixtures of DME and H_2O, we express the interconversion as hydrolysis of DME to form MeOH (Reaction [Rxn.] 1):

$$CH_3OCH_3 + H_2O \rightleftharpoons 2\ CH_3OH. \qquad \textbf{[Rxn. 1]}$$

As a consequence, under typical MTH conditions, not only MeOH but also DME and H_2O are present in the feed. The gas-phase composition is determined by the initial composition of the feed and the MeOH–DME interconversion (Rxn. **1**) but also (as the MTH reaction progresses) by the different rate of consumption of MeOH and DME in the formation of hydrocarbons. We have observed that before methylation reactions become dominant the concentrations of MeOH, DME, and H_2O remain constant in a relatively broad contact time range (broader for higher concentrations of H_2O; *SI Appendix*, Fig. 1). These concentrations of MeOH, DME, and H_2O indicate that interconversion between MeOH and DME is equilibrated. We have quantified the approach to equilibrium for different feed compositions as a function of contact time. Because our starting point is dry DME mixed with increasing concentrations of H_2O, we define the approach to equilibrium for Rxn. **1**, i.e., DME hydrolysis. The deviation of the system from equilibrium can be better examined by the use of the approach-to-equilibrium value η_{eq} of the reverse of Rxn. **1** (Fig. 2A):

$$\eta_{eq} = \frac{P_M^2}{P_D P_W} / K_{eq}. \qquad \textbf{[1]}$$

In Eq. **1**, MeOH, DME, and H_2O are assumed to behave ideally. The MeOH/DME conversion in Fig. 2A follows the characteristic S-shape curve with contact time, with an initiation zone ranging from 0 to 0.05 $min \cdot kg_{cat} \cdot mol_{total\ carbon}^{-1}$ and autocatalysis zone from 0.05 to 0.15 $min \cdot kg_{cat} \cdot mol_{total\ carbon}^{-1}$. Fig. 2A also shows the approach to equilibrium and the partial pressures of MeOH, H_2O, and DME measured for a reaction with initial feed of 90 mbar DME and 90 mbar water on H-ZSM-5 (*SI Appendix, section 1* for details). It can be seen that MeOH, DME, and H_2O quickly reached steady partial pressures at short contact times (*ca.* 0.025 $min \cdot kg_{cat} \cdot mol_{total\ carbon}^{-1}$), with a calculated pseudoequilibrium constant of $P_M^2/(P_D P_W) = 0.201 \pm 0.004$, in which P_M,
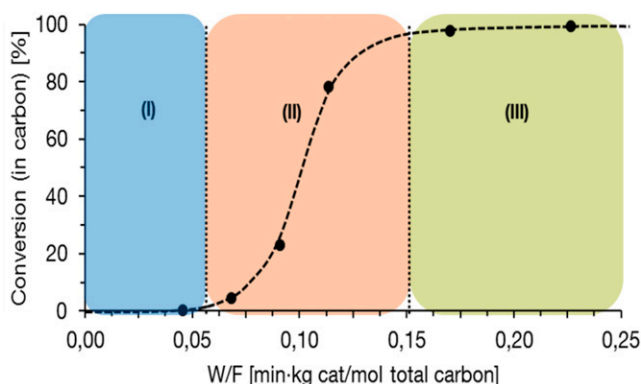
Fig. 1. Reaction stages in the methanol conversion to hydrocarbons as a function of contact time (W/F). Methanol conversion curve with contact time showing the typical S-shape profile for autocatalytic reactions. The different reaction stages that develop as a result of the change in nature of gas phase composition from oxygenates to hydrocarbon + H_2O with conversion is marked by dashed lines. (I) Initiation stage, (II) methylation stage, and (III) hydrocarbon interconversion stage.
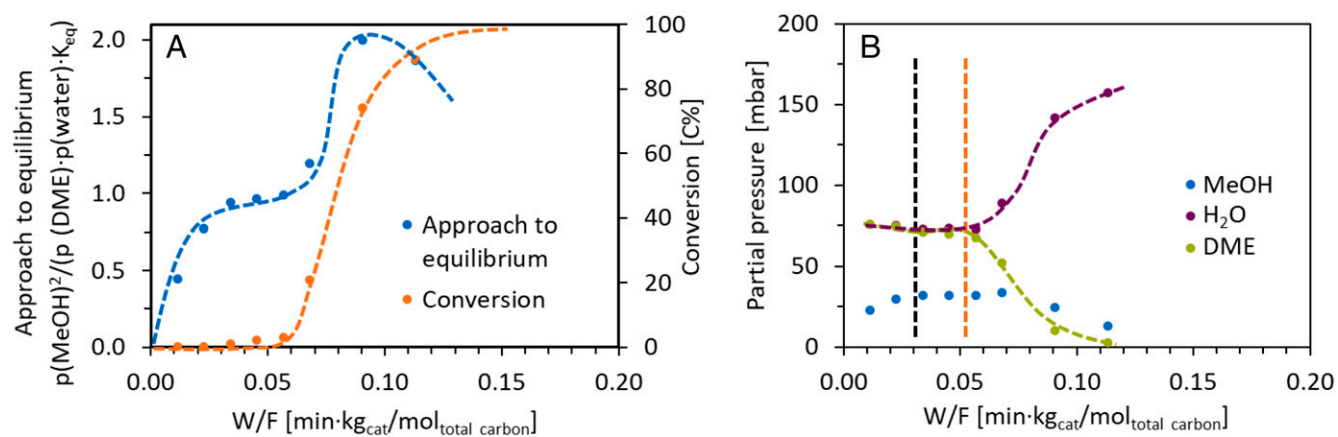
Fig. 2. Methanol dehydration equilibrium and evolution of oxygenates in the outlet as a function of contact time (W/F). (*A*) gives approach to equilibrium defined as $[P_M^2/(P_D P_W)]/K_{eq}$ as well as the overall conversion of DME and MeOH. (*B*) depicts the partial pressure of DME and MeOH measured in the outlet, and partial pressure of H_2O calculated by assuming an average of four C atoms in the hydrocarbon products. The black dashed line marks the contact time at which 0.02 C % propene is observed, and the orange dashed line the point at which the approach to equilibrium diverges from 1. Reaction conditions: T = 748 K, Feed: N_2/DME/H_2O, pressure at inlet p (DME) = 90 mbar, p (H_2O) = 90 mbar.

P_D, and P_w are the pressure of MeOH, DME, and water, respectively. It should be noted that at very short contact time (0.01 min·kg$_{cat}$/mol$_{total\ carbon}$ in this case), the partial pressures of MeOH, DME, and H_2O are already close to the equilibrium composition. However, due to the bimolecular nature of the reaction, a P_M deviation of 20% translates into an approach to equilibrium of only *ca.* 0.5.

On the other hand, after the onset of alkene formation, MeOH and DME are rapidly consumed (and H_2O produced) due to the fast autocatalytic conversion either via alkene (olefin pathway) or via arene (aromatics pathway) alkylation. For the case illustrated in Fig. 2, this occurs at contact times above 0.05 min·kg$_{cat}$/mol$_{total\ carbon}$, as marked by the dashed orange line. Once these reactions become faster than the rates leading to interconversion of MeOH, DME, and H_2O the partial pressures of these molecules are no longer equilibrated at the reactor outlet.

In order to obtain kinetic parameters of the rate-limiting reaction in the first C–C bond formation and related reactions during the first stages of the MTH conversion, we establish that the reaction conditions applied should ensure equilibration of MeOH, DME, and H_2O. Therefore, for each feed composition we determine the range of contact time at which approach to equilibrium is *ca.* 1 and, simultaneously, the yield of hydrocarbon products, represented by the first-most-abundant product detected propene, is below 0.02% C. In Fig. 2*B*, we can see that setting a limitation of the hydrocarbon yields to <0.02% C (black dashed line) is more restrictive than the equilibration of DME and MeOH. In other words, by establishing the hydrocarbon yields upper limit to 0.02% C we conservatively impose reaction conditions at which the equilibration of DME, MeOH, and H_2O is ensured in all conditions tested in this work.

CH$_4$ Formation as Primary Product of DME and MeOH on ZSM-5

Besides the interconversion of MeOH and DME via dehydration and hydrolysis, small concentrations of CH$_4$, HCHO, and CO form in the initiation stage of the MTH conversion. In the absence of other hydrocarbon products or intermediates, these C$_1$ molecules are hypothesized to form via hydrogen transfer from MeOH to a methoxy group formed from dissociative adsorption of methanol (25, 26).

Regardless of the mechanism, an overall reaction of methanol to formaldehyde and methane should lead to equimolar quantities of both products:
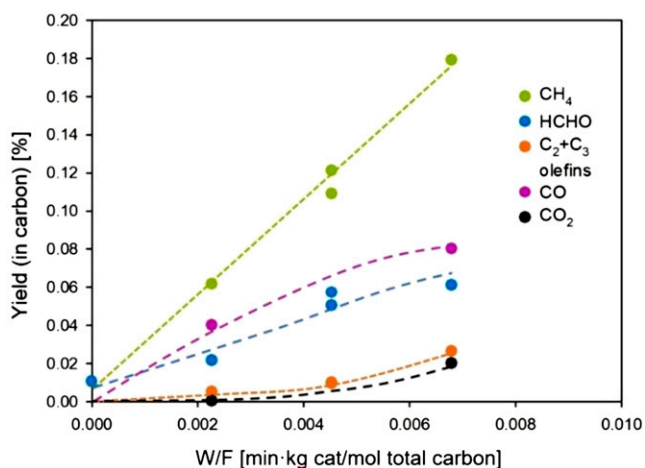
$$2\ CH_3OH \rightarrow CH_4 + HCHO + H_2O. \qquad \textbf{[Rxn. 2]}$$

Formation of CH$_4$ and formaldehyde from methanol as in Rxn. **2** is a crucial step in the methane–formaldehyde mechanism proposed by Tajima et al. (27), where a C–C bond is subsequently formed between CH$_4$ and formaldehyde. Hydride transfer from DME or methanol to a methoxy group is also the first step in the formation of CO, which can be then subsequently methylated, which has been shown to be more favorable than the methane–formaldehyde mechanism (28). Even though it occurs at very low rates, the formation of HCHO and CO initiated by Rxn. **2** is widely accepted as a key step for the formation of the first alkenes that are subsequently transformed to higher hydrocarbons (hydrocarbon pool) (18, 21–23).

Previous reports (29) had concluded that only MeOH may lead to formaldehyde under MTO conditions. However, our experiments with dry DME reacting on H-ZSM-5 at very short contact times (up to 0.007 min·kg$_{cat}$·mol$_{total\ carbon}$$^{-1}$) and low conversions (<0.3 C%) also lead to CH$_4$, HCHO, CO, and CO$_2$ (Fig. 3). Formation of H$_2$ was also observed but could not be quantified. Under these (dry) conditions, the presence of MeOH is ruled out. It can be seen that CH$_4$, HCHO, and CO are the main gaseous products from DME. In a blank test (data point at W/F = 0) equimolar quantities of CH$_4$ and HCHO were formed (*ca.* 0.01%C), indicating a small contribution from thermal decomposition. CH$_4$ is clearly a primary product of DME and we propose its formation via decomposition of DME with concomitant formation of one molecule of HCHO (Rxn. **3**). This decomposition (Rxn. **3**) has been mentioned in two earlier contributions (15, 28):

$$CH_3OCH_3 \rightarrow CH_4 + HCHO. \qquad \textbf{[Rxn. 3]}$$

As shown in Fig. 3, a very small amount of C$_2$ and C$_3$ olefins appeared in the DME reaction on ZSM-5 at ~0.005 min·kg$_{cat}$·mol$_{total\ carbon}$$^{-1}$. These short alkenes are the main C–C bond containing products under those conditions. The methane yield increased linearly from the beginning of the reaction, until the formation rate of olefins started to increase significantly (from 0.007 min kg$_{cat}$·mol$_{total\ carbon}$$^{-1}$ on). This points to a constant formation rate of methane in the initiation period.

Based on Rxns. **2** and **3**, HCHO should be formed in equimolar amounts to CH$_4$. However, measured HCHO formation rates were lower than those to CH$_4$. This difference is attributed to the high reactivity of HCHO, which leads to its rapid consumption in consecutive chemistries, such as the decomposition

CHEMISTRY

Fig. 3. Yield of C_1 products and lumped $C_2 + C_3$ olefins at short contact times. Reaction conditions: T = 748 K, Feed: N_2/DME, p (DME) = 90 mbar; $\dot{n}$ (C-based) = 14 mmol/h. Data at zero W/F are from blank reaction carried out in presence of SiC only.

to CO or the condensation with surface species to build the hydrocarbon pool (18, 19, 23, 28, 30, 31). It should be noted that for the gas products detected in the conditions of Fig. 3 the C and O balance are closed and, therefore, the accumulation of hydrocarbons or oxygenates strongly adsorbed on the zeolite surface can be neglected.

In contrast to the high reactivity of HCHO in secondary reactions, CH_4 is stable and inert on H-ZSM-5 under the applied MTO conditions. Even cofeeding 167 mbar CH_4 with DME did not promote its reaction (*SI Appendix*, Table 2) and therefore it can be considered to be an end-product. At these low conversions, one can exclude the contribution of reaction pathways other than Rxns. **2** and **3** to CH_4 formation. Especially, formation of CH_4 by cracking of hydrocarbons from the emerging hydrocarbon pool and from coke deposits that have been reported at higher conversions (32, 33) is negligible under the reaction conditions discussed here. This is shown by the fact that catalyst tested under low conversions led to the same CH_4 yield even after being exposed to space velocities where the hydrocarbon pool was allowed to fully develop and the catalyst even converted 20% of DME (*SI Appendix*, Fig. 2). On the other hand, because CH_4 was the only alkane observed under the studied conditions, we rule out any significant contribution to HCHO formation from the methanol-induced hydrogen transfer (34) to larger carbenium ions.

The evolution of the methane yield with contact time in the initiation stage of MTO (region I in Fig. 1) was monitored for different feed compositions. In all cases, a linear increase of the CH_4 yield with contact time was observed with the slope representing the CH_4 formation rate (*SI Appendix*, section 2 and Fig. 3). This indicates that CH_4 is a primary and stable product of MeOH and DME on H-ZSM-5.

Based on all experimental evidence, we conclude that the CH_4 formation rate at low conversions is a suitable quantitative descriptor of the formation rate of HCHO from DME/MeOH feeds, because all the possible CH_4 formation pathways entail the formation of equimolar quantities of HCHO (Rxns. **2** and **3**).

Kinetics of CH_4 Formation, as a Proxy for HCHO Formation, in the Initiation Stage of MTH Conversion
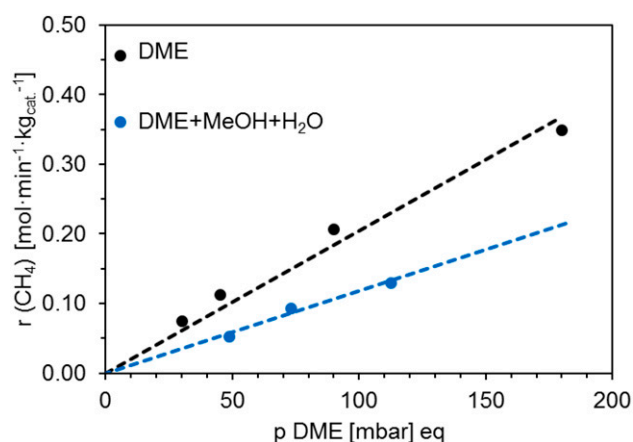
Determining the reaction kinetics for CH_4 formation as a function of the chemical potential of the three feed components (DME, methanol, and water) is the basis for further understanding of the reaction mechanism of oxygenates in the

initiation stage. However, due to the fast interconversion between MeOH, DME, and water (Rxn. **1**), it is not possible to independently vary their partial pressures. In order to ensure a stable and well-defined feed composition for the kinetic study of methane formation, we only use data in the contact time range, for which quasi-equilibration of Rxn. **1** is achieved (i.e., between 0.020 and 0.055 $min \cdot kg_{cat} \cdot mol_{total\ carbon}^{-1}$ in Fig. 2). It should be noted that such a contact time range varies with H_2O content in the feed and must be adjusted for each condition (*SI Appendix*, section 1). In the selected contact time region, the partial pressure of one of the three feed components can be kept constant by adjusting the overall flow with an inert gas (N_2), while the other two vary accordingly to their equilibrium.
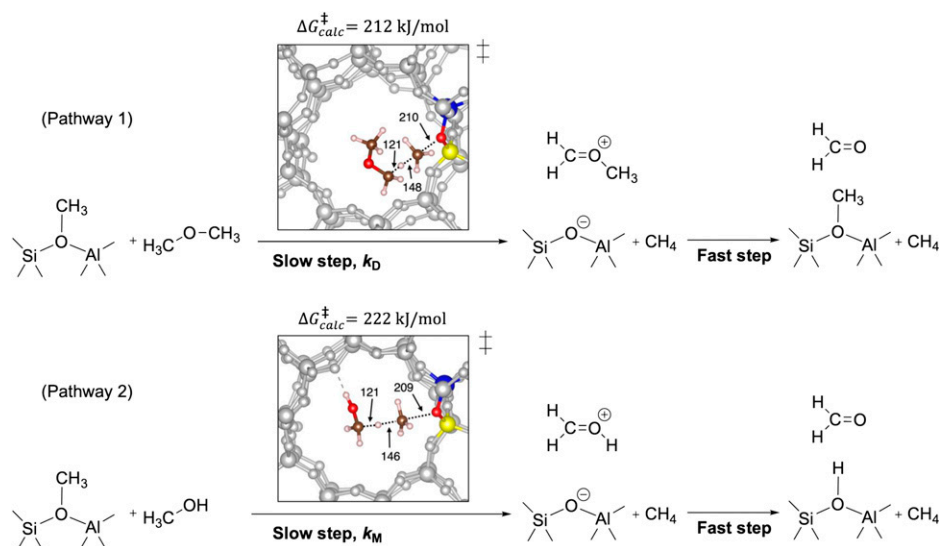
The reaction with dry DME is the simplest case. In the absence of H_2O, hydrolysis of DME to MeOH (Rxn. **1**) is excluded and the formation rate of methane is only related to reactions from DME. The CH_4 formation rate increased proportionally with increasing DME pressure (Fig. 4, black line), indicating a first-order reaction with respect to DME (*SI Appendix*, Fig. 4). This indicates that a surface reaction exists in which DME is converted to CH_4 and HCHO (Rxn. **3**).

Next, we cofed DME and H_2O in a N_2 flow under reaction conditions similar to the experiments in absence of water. Under these conditions MeOH, DME, and H_2O quasi-equilibrate at very short contact times. Based on this quasi-equilibration, we adjusted the DME and H_2O partial pressures in the feed in order to reach constant MeOH partial pressure for all measurements in Fig. 4. The measured CH_4 formation rate in this contact time range (Fig. 4, blue line and *SI Appendix*, Table 3) was significantly lower than the rate obtained with dry DME. The reaction order of ~1 in DME was preserved, despite the presence of different concentrations of H_2O (*SI Appendix*, Fig. 5A). With constant DME pressure, the methane formation rate decreased with increasing MeOH and H_2O partial pressures, showing a negative reaction order of −0.59 for MeOH (*SI Appendix*, Fig. 5B).

We hypothesize that at low conversions only two possible reaction pathways of DME and MeOH exist that could lead to CH_4: hydrogen transfer from DME to surface methoxy species (SMS), as shown in Fig. 5, Pathway 1 and hydrogen transfer from MeOH to SMS as shown in Fig. 5, Pathway 2. The direct

Fig. 4. Methane formation rate as a function of DME pressure. Pure DME feedings shown in black and mixtures of DME, MeOH, and water in blue. In the latter case feed conditions are chosen to reach a constant MeOH partial pressure of *ca.* 34 mbar via Rxn. **1** equilibration, while the water partial pressures increase parallel to the DME partial pressures. Reaction at 748 K and partial pressures of the feed as shown in *SI Appendix*, Table 3. Rates calculated in the contact time range where DME and MeOH interconversion can be regarded as equilibrated (*SI Appendix*, section 1 for details).

Fig. 5. Postulated reaction pathways for decomposition of DME and MeOH into methane and formaldehyde, with transition states and energetic barriers as calculated by density functional theory. The atomic structure of the computed transition states is shown (color code: H: white, C: brown, O: red, Si: yellow, Al: blue, remaining framework: gray) and selected bond lengths are indicated in picometers.

decomposition of DME on BAS to form CH_4 and HCHO is concluded to be unlikely, as will be discussed below. Other routes leading to CH_4, such as cracking or hydrogen transfer from entrained hydrocarbons or coke, can be ruled out under the current reaction conditions.

Previous work has shown that the formation of CH_4 and HCHO from DME via Pathway 1 is energetically feasible on H-SSZ-13 (28). In order to shed light on the reaction of methanol and DME with BAS and with SMS on ZSM-5, we turned to computations of the mechanistic pathways, focusing on Scheme 1 for the T12 site of H-ZSM-5 using periodic density functional theory calculations employing the Perdew–Burke–Ernzerhof (PBE) functional with dispersion corrections (D3) in conjunction with highly accurate ab initio calculations on cluster models (see *Methods*). Free energies were computed at 748 K and 1 bar reference pressure. As shown in Fig. 5, the reaction of MeOH with an SMS leading to the formation of formaldehyde and methane has a free energy barrier of 222 kJ/mol. For DME, the analogous formation of formaldehyde and methane via reaction at an SMS has a lower barrier of 212 kJ/mol. We have additionally investigated H_2 formation both from methanol and DME (*SI Appendix*, Fig. 10) and found the corresponding barriers to be 232 and 254 kJ/mol, respectively, thus being significantly higher than for CH_4 formation. Our calculations suggest that the direct decomposition of

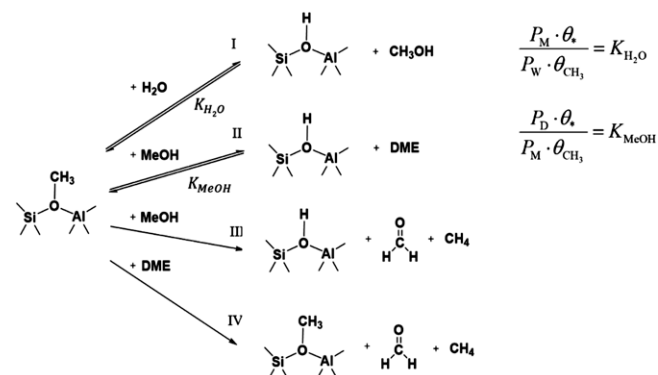DME on BAS to form CH_4 and CHOH without mediation of methoxy species is not favorable. Attempts to locate transition states for this mechanism instead lead to different reactions, such as the production of H_2.

For the hydrogen transfer in Pathways 1 and 2, we propose the reaction network linked by surface methoxy species in Scheme 1, including the formation of methoxy and CH_4 from DME and MeOH in the initiation zone, and the concomitant generation of key intermediates for the formation of C–C products (i.e., formaldehyde). The reactions (I) and (II) in Scheme 1 are proposed to be elementary steps in the interconversion of DME and MeOH (Rxn. **1**) on H-ZSM5 at 748 K, with methoxy species as main surface intermediates (35). We only considered CH_4 formation via surface methoxy species and not via adsorbed methanol, because the latter type of mechanism is known to become unfavorable at high temperatures due to the associated entropic loss. For example, Jones and Iglesia have predicted the cross-over in methanol dehydration rates from direct to stepwise mechanism to occur at 503 K for 0.1 bar of methanol (20).
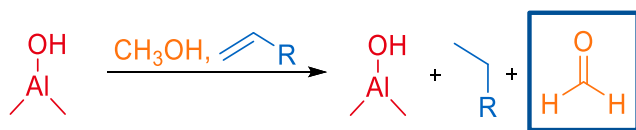
As mentioned above, the gas phase composition of MeOH, DME, and H_2O is equilibrated in most of the initiation stage (Fig. 2 and *SI Appendix*, section 1). Therefore, at the reaction conditions used here (T = 748 K, conversions <0.8 C%) it is hypothesized that the transformation of BAS into methoxy species is determined by the reaction pseudoequilibria I and II in Scheme 1 (20).

According to Scheme 1, the reaction of SMS with methanol leads either reversibly to DME (Reaction II) or quasi-irreversibly to formaldehyde and methane via hydrogen transfer (Reaction III). It should be noted that the reaction of SMS with H_2O forms methanol and restores a BAS (Scheme 2, Reaction I). Thus, the water partial pressure influences not only the partial pressure of MeOH and DME by Rxn. **1** but also the available concentration of reactive surface methoxy species, which are relevant for Pathways 1 and 2 in Fig. 5.

In the proposed reaction pathway of Scheme 1, the hydrogen transfer from DME or MeOH to surface methoxy species is the rate-determining step (reactions III and IV) for CH_4 formation. The consumption of MeOH, DME, or methoxy species via buildup of a hydrocarbon pool or via methylation of C–C-containing intermediates is hypothesized to be negligible under

Scheme 1. Reaction pathways starting from surface methoxy species and the feed components MeOH and H_2O.

$$\frac{P_M \cdot \theta_*}{P_W \cdot \theta_{CH_3}} = K_{H_2O}$$

$$\frac{P_D \cdot \theta_*}{P_M \cdot \theta_{CH_3}} = K_{MeOH}$$

Scheme 2. The hydrogen transfer between methanol and an alkene molecule to form formaldehyde and an alkane molecule, catalyzed over extra-framework Al-related Lewis acid sites (Al-OH) (34).

these reaction conditions. We base this assumption on 1) the very small amounts of C–C products detected (upper limit set at 0.02% C propene for the kinetic study), 2) the short time on stream (TOS) at which data were collected (10 to 20 min), and 3) the closed C balance of products at these low conversions (Fig. 3).

According to the adsorption entropy and enthalpy values reported by us (36), Pope (37) and Piccini et al. (38) calculated that the coverage of BAS by H_2O (θ_W), MeOH (θ_M), and DME (θ_D) can be regarded as negligible at 748 K, i.e., $\theta_W \approx \theta_M \approx \theta_D \approx 0$ (*SI Appendix*, section 3.1). As mentioned above, also the influence of hydrocarbon buildup can be disregarded under the low conversions applied here. Thus, we hypothesize that in the MTH initiation stage the only surface species to be considered are methoxy groups at bridging lattice oxygen. Under this assumption, the coverage is solely affected by the four reactions shown in Scheme 1.

In the initiation stage, the methane formation rate r_{CH4} is contributed by Reactions III and IV in Scheme 1, with each rate being proportional to surface methoxy coverage (θ_{CH3}) and pressure of MeOH (P_M) or DME (P_D):

$$r_{CH_4}(III) = k_M \theta_{CH_3} P_M \qquad [2a]$$

$$r_{CH_4}(IV) = k_D \theta_{CH_3} P_D. \qquad [2b]$$

Here, k_D and k_M refer to the reaction rate constants for the methane formation from DME and MeOH, respectively, Reactions IV and III in Scheme 1. The total methane rate is the sum of the two and can be expressed as Eq. 2, in which P_W is the pressure of water (*SI Appendix*, sections 1 and 3 for details):

$$r_{CH_4} = \frac{P_M}{P_W K_{H_2O} + P_M} \cdot (k_D P_D + k_M P_M). \qquad [3]$$

For the special case of the reaction of dry DME at low conversion levels ($P_W \to 0$ and $P_M \to 0$), r_{CH4} in Eq. 3 is approximated to (*SI Appendix*, section 3.2)

$$r_{CH_4} \approx k_D P_D. \qquad [4]$$

This approximation is in good agreement with the observed proportional increase of the methane rate with DME pressure (reaction order 1) in Fig. 4. Fitting the data with Eq. 4 gives a value of k_D of 2.1 ± 0.2 mol·min^{-1}·kg$_{cat}^{-1}$·bar^{-1}.

To determine the values of k_M and K_{H_2O}, Eq. 3 is rearranged into

$$P_M(r_{CH_4} - k_D P_D) = k_M \cdot P_M^2 - K_{H_2O} \cdot r_{CH_4} P_W. \qquad [5]$$

With the rates at different MeOH, DME, and H_2O pressure (*SI Appendix*, Table 3), experimental data for $P_M \cdot (r_{CH4} - k_D \cdot P_D)$, P_M^2 and $r_{CH4} \cdot P_W$ can be displayed as a surface in a three-dimensional plot (*SI Appendix*, Fig. 7). The excellent fit of the data to Eq. 4 with $R = 0.96$ validates the proposal of reaction network in Scheme 1 and the approximations taken for the kinetic analysis of the initiation stage. The regression led to a reaction rate constant k_M of 0.15 ± 0.15 mol·min^{-1}·kg$_{cat}^{-1}$ bar^{-1} and pseudoequilibrium constants K_{H_2O} of 0.37 ± 0.08 (*SI Appendix*, Table 4). The rate constant k_D is one order of magnitude higher than k_M. Therefore, we conclude that the main route of CH_4 (and HCHO) formation in the initiation stage of
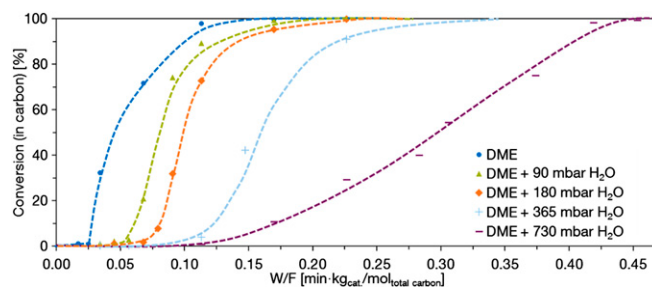
methanol conversion to hydrocarbons is the hydrogen transfer from DME to SMS (Pathway 1). From our experimental data fitting to Eq. 5 we obtain $\Delta G^{\circ\ddagger}$ values for MeOH and DME at 748 K of 210 kJ/mol and 193 kJ/mol, respectively. This barrier difference of 17 kJ/mol is in good agreement with the 10 kJ/mol difference predicted by our theoretical calculations.

Consequences of Hydrogen Transfer Rates for the Formation of the Hydrocarbon Pool

Fig. 6 shows the conversion of DME/MeOH under different DME and water cofeeding compositions. Because the rate of hydrogen transfer from DME and MeOH to methoxy groups is proposed to be the rate-determining step for the overall Rxns. 2 and 3, the rate of formation of CH_4 via reactions III and IV in Scheme 1 is set equal to the rate of formation of formaldehyde. It should be emphasized again that HCHO is considered a key intermediate in the initiation reactions for the formation of hydrocarbons (18, 21–23). Then, according to our mechanistic proposal, at lower partial pressures of H_2O a faster formation of the hydrocarbon pool is expected—via reaction of DME to form HCHO—reducing the contact time required to reach the onset of olefin formation. In good agreement, Fig. 6 shows that the presence of increasing concentrations of H_2O in the feed increases the contact time necessary to trigger the formation of hydrocarbons.

The initial formation rate of the hydrocarbon pool cannot be directly measured in the kinetic experiments, but an indirect quantification is provided by examining the minimum contact time necessary to initiate the autocatalytic MTO reaction. As a criterion for the transition from initiation to methylation, we select the contact time at which 0.02 C % of propene is generated as indicator, and we name it the "critical contact time." This indicator is chosen because at these low conversions $C_3^=$ and $C_2^=$ are the main C–C-containing products and only traces of higher alkenes or aromatics are detected. On the other hand, the MeOH/DME conversion curve rapidly increases at $C_3^=$ yields above 0.05% C.

Fig. 7 shows that the critical contact time increased with increasing water content in the feed. For the highest tested H_2O partial pressure (730 mbar), the critical contact time was about four times larger than for dry DME. The critical contact time correlates excellently with the methane formation rates during the initiation period, regardless of the H_2O content of the feed (Fig. 7A). Thus, the critical contact time is concluded to be inversely proportional to the C_1 hydrogen transfer rate. A pseudorate of formation of the hydrocarbon pool can, thus, be derived from the critical contact time values (Eq. 6):

Fig. 6. Conversion of MeOH and DME at 748 K under different feed compositions versus contact time. DME partial pressure in the inlet is kept constant at 90 mbar. The MeOH/DME/H_2O reacting mixture composition after equilibration can be found in *SI Appendix*, Table 3. Curve obtained with pure MeOH is shown for comparison in *SI Appendix*, Fig. 8. W/F is defined by the total molar amount of introduced carbon, which is kept constant during all measurements, while the catalyst loadings are varied for each measurement.
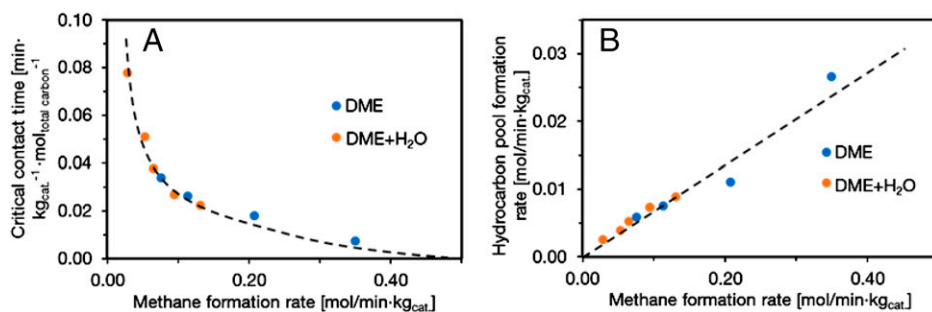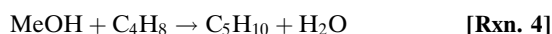
Fig. 7. Correlation between CH_4 formation rates and hydrocarbon pool formation. Correlation between the methane formation rate and (*A*) the critical contact time to initiate the methylation stage (defined by the formation of 0.02 C % of $C_3^=$) and (*B*) the pseudo rate of hydrocarbon pool formation based on apparent $C_3^=$ formation. "DME" marks measurements where the feed is dry DME in N_2 dilution, while "DME+H_2O" denotes measurements where different DME/water mixtures in N_2 were used as feed. All measurements at 748 K.

$$r_{\text{Hydrocarbon pool formation}} = \frac{0.0002\ (mol_{propene}/mol_{total\ carbon})}{Critical\ contact\ time\ (\min \cdot kg_{cat}/mol_{total\ carbon})}.$$

[6]

This pseudo rate of hydrocarbon pool formation is directly proportional to the CH_4 formation rate (Fig. 7*B*). Based on our own results and literature, CO and HCHO are involved in several pathways to start forming the hydrocarbon pool (22, 23, 27, 28). The correlation depicted in Fig. 7*B* supports these proposals, suggesting that the kinetically relevant step in the formation of the first C–C products is identical to the rate of CH_4 formation, which is stoichiometrically linked to HCHO (and CO). Thus, one can conclude that the rate-determining step of the hydrocarbon pool formation is proportional to the formation rate of HCHO (and CO), i.e., the hydrogen transfer between DME or MeOH and surface methoxy species to generate the C_1 reaction intermediates. It should be noted that our data cannot rule out the coexistence of other proposed mechanisms for formation of the first C–C bond such as those mediated by carbene species (23, 39). However, the correlation between CH_4 formation and C–C bond formation is a strong indication that the formaldehyde-mediated mechanism dominates the MTH kinetics in the initiation stage.

Effects of H_2O Partial Pressure on Methylation and the Dual-Cycle Mechanism

Experimentally, the absolute methylation rates observed for MeOH feeds are lower than for DME feeds (9, 15). Accordingly, in Fig. 6 we observed a decrease in the slope of the conversion curve (in the 10 to 90% conversion range) when the H_2O content increased. In this conversion range (methylation stage, II in Fig. 1), as soon as a critical concentration of alkenes is formed, the continuous propagation of the dual (olefin and aromatics) cycle sets in. In the dual cycle, DME and MeOH are rapidly consumed via methylation of alkenes and arenes in the olefin and aromatic cycle, respectively. The rates of these methylation reactions are orders of magnitude higher than the reactions initiating the hydrocarbon pool, which results in the S-shape of the MeOH/DME-conversion curves in Figs. 2*A* and 6. The methylation of an alkene (e.g., butene) or an aromatic ring with MeOH generates one H_2O molecule per MeOH consumed (Rxn. **4**). Conversely, methylation via DME stoichiometrically generates a molecule of MeOH (Rxn. **5**):

$$MeOH + C_4H_8 \rightarrow C_5H_{10} + H_2O \qquad \textbf{[Rxn. 4]}$$

$$DME + C_4H_8 \rightarrow C_5H_{10} + MeOH. \qquad \textbf{[Rxn. 5]}$$

As soon as the dual cycle propagates, the concentration of hydrocarbons in the zeolite pores increases and the methylation

Rxns. **4** and **5** become faster than the interconversion of DME and MeOH (Rxn. **1**). Under such conditions, it is not possible to apply conventional kinetic analysis to calculate a net methylation rate from experimental data. However, we note that examining the evolution of DME/MeOH/H_2O partial pressures in the first stages of methylation, the initial consumption rate of DME is much larger than that of MeOH, the latter being close to zero (Fig. 2*B*). Given that methylation with DME as in Rxn. **5** generates 1 mol of MeOH per mole of reacted DME, the relatively constant MeOH concentration to conversions even above 50% (Fig. 2*B*) indicates that Rxns. **4** and **5** have rates in the same order of magnitude. We conclude that methylation rates in the 10 to 50% region are dependent on the concentration of surface methoxy species, regardless of the nature of the oxygenate in the gas phase.

In addition to methylation Rxns. **4** and **5**, the formation of hydrogen transfer products (aromatics and alkanes) becomes also significant in the educt stream already in the conversion range of 1 to 10%. Previous studies have shown that at low oxygenate conversions the dominant pathway for the formation of aromatics and alkanes in ZSM-5 is the hydrogen transfer from methanol to an alkene molecule (so-called methanol-induced hydrogen transfer [MIHT], Scheme 2) (34).

In this mechanism, hydrogen transfer from MeOH to an olefin generates highly reactive HCHO and an alkane. The subsequent reaction of HCHO with olefins generates aromatics via the Prins reaction (18). At medium conversions (stage II in Fig. 1) it is not possible to differentiate between the net contribution of DME and MeOH to this type of hydride transfer. While evaluating the rate constants is not possible due to the unknown concentration of hydrocarbons, the overall alkane formation rate in the different stages of MTO conversion for different DME/H_2O feeds can be determined (*SI Appendix*, Fig. 9). In agreement with the lower hydride transfer rate of MeOH compared to DME in their reaction with methoxy species (stage I), $C_{1–4}$ alkane formation rates at partial MTO conversions via hydride transfer of oxygenates to alkenes (stage II) also decrease with the H_2O partial pressure, i.e., with increasing concentration of MeOH in the feed. Once full conversion is achieved the rate of formation of alkanes is similar regardless the concentration of water in the feed.

Fig. 8 compares the effect of feed H_2O content in the methylation rates, calculated as the combined consumption of methanol and DME, and in the MIHT rates calculated as formation rate of aromatics and $C_{1–4}$ alkanes. Stepwise methylation is accepted as the dominant mechanism for alkene formation at these low conversions (40, 41). In this mechanism, methoxy species are the key surface intermediates and methylations occur via nucleophilic attack of an alkene or an aromatic ring on a surface methoxy species. The presence of water reduces the surface
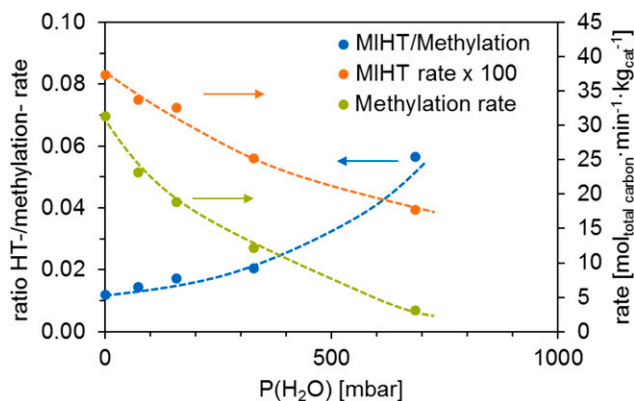
Fig. 8. Effect of H_2O partial pressures in rates of methylation and methanol-induced hydrogen transfer reactions. Correlation of the ratio between the MIHT rate and the methylation rate with the water partial pressure in the equilibrium. All rates are determined at 748 K and in the region between 5 and 30 C % conversion.

concentration of methoxy groups on BAS (Scheme 1, I) and, hence, decreases the concentration of potential transition states and lowers the observed overall methylation rate.

In Fig. 8 it can be seen that as the water partial pressure increased the rate of formation of aromatics and alkanes (represented as MIHT rate) decreased. As shown in Scheme 2, the rate-determining step of the MIHT pathway have been proposed to be the formaldehyde formation on LAS and does not involve SMS or BAS (34). Although this mechanism was originally proposed for MeOH as reactant, there is no evidence against a reaction starting from DME under H_2O-poor conditions. Therefore, we hypothesize that the negative effect of H_2O on this rate is related to an overall higher reactivity of DME for hydrogen transfer.

The presence of water is known to impact the product selectivity of MTH (6, 7, 9). In Fig. 8, it is also shown how the MIHT-to-methylation-rate ratio changes with H_2O partial pressure. Although both rates decreased in presence of H_2O, the effect was stronger for the methylation pathway, causing the MIHT/methylation ratio to increase. As a consequence, higher selectivities to alkanes and aromatics can be expected at elevated H_2O partial pressures. This is in good agreement with other studies that have reported lower alkane and aromatic yields, when DME was used as reactant instead of MeOH (9). Consequently, the overall catalyst lifetime is expected to decrease with increasing H_2O content (9, 10, 16). Although this effect was already observed and described in the abundant MTH literature, we demonstrate here that its cause is not related to a lower reactivity of DME to hydrogen transfer reactions. On the contrary, the negative impact of H_2O (and with it the higher concentration of methanol) on the individual rates of C–C bond formation, methylation, and formation of alkanes and aromatics is the combined result of the concentration of surface methoxy species—regulated by the presence of H_2O and the hydrolysis of SMS to restore BAS—and the higher reactivity of DME for hydrogen transfer reactions, i.e., about one order of magnitude for the measurable case of hydrogen transfer to methoxy species.

Conclusions

The experiments and theory reported here provide a mechanistic understanding of the effect of H_2O on rates and selectivities of zeolites such as ZSM-5 for methanol conversion to hydrocarbons. Reaction conditions leading to very low conversions allow us to eliminate the interference of the fast and mechanistically

dominant methylation of hydrocarbons and of associated subsequent reactions. In this way, kinetic information of the reactivity of oxygenates on zeolites that was hitherto not available becomes experimentally accessible. In the initiation stage of the autocatalytic conversion of MTH, both DME and MeOH are found to react to C_1 intermediates that trigger the C–C bond formation on ZSM-5. Among the different possible reaction pathways, kinetic analysis and ab initio calculations show that the dominant reaction is the hydride transfer from DME to methoxy groups formed on zeolite BAS to produce HCHO and CH_4. This hydride transfer step is one order of magnitude faster than hydride transfer from methanol, i.e., dimethyl ether is the stronger hydrogen donor to methoxy species than MeOH. The strictly linear correlation between the rate of hydrocarbon pool formation and of methane formation allows us to conclude that the hydride transfer step leading to formaldehyde and CO is rate-determining for the initial C–C bond formation that starts the autocatalytic MTO conversion.

Once a threshold concentration of species in the hydrocarbon pool is formed, the methylation reactions become dominant. In the low contact time regime (hydrocarbon interconversions negligible), however, the net methylation rate does not depend on the partial pressure of MeOH or DME but on the population of surface methoxy intermediates. Because the overall rate of methylation decreased sharply with increasing H_2O partial pressures, we conclude that H_2O reduces the coverage of methoxy species via hydrolysis, restoring BAS and reducing both the methylation rate and the formation rate of C_1 species, by reducing the concentration of potential sites for hydride transfer.

The rate of formation of nonolefinic by-products, i.e., alkanes and aromatics, also decreases with increasing water partial pressure for medium conversions. We hypothesize that the alkane and aromatics formation rates decrease with H_2O content because of the higher reactivity of DME in comparison to MeOH for hydrogen transfer to alkenes. Due to the lesser effect of H_2O on the hydrogen transfer rates, the methylation/hydrogen transfer rates ratio decreases with H_2O partial pressure and therefore the selectivity toward aromatics and alkanes increases.

A better understanding of these elementary steps involved in the MTH reaction and their dependence on the feed composition is fundamental to improve catalyst properties and to guide operations of the process. Here it is shown that the different reactivity of DME and MeOH in hydrogen transfer reactions and the concentration of surface methoxy species as main active species in H-ZSM-5 in presence of oxygenates determine the catalytic activity. Hydride transfer of DME and MeOH determines the formation rate of formaldehyde and in consequence its chemical potential, acting as key intermediate in both activation and deactivation during MTH conversion in zeolites. The quantitative measure of hydrogen transfer kinetics of oxygenates and its relationship with Brønsted and Lewis acid sites and surface species serves as an additional tool to adjust product distribution and predict the lifetime of a MTH catalyst based on the H_2O content of the feed.

Methods

Materials. H-ZSM-5 catalyst has an Si/Al ratio of 90 and was synthesized according to the procedure described by Ong et al. (42). Further details on the preparation are provided in *SI Appendix*. Methanol (≥99.9%) and DME (≥99.9%) were supplied by Sigma-Aldrich. The introduced deionized water was further purified by an EASYpure II RF-Compact-Waterfilter by Barnstead.

Computational Methods. A periodic model of H-ZSM-5 was employed with an Al/Si ratio of 1/95, where one Al atom per unit cell is located in the T12 position. The lattice constants were taken from previous work (43) and were kept fixed in all calculations in this work. Periodic PBE-D3 calculations (44, 45) were performed with the projector augmented wave (PAW) method as implemented in the VASP program package (46, 47) in version 5.4.1, appropriate PAW potentials and an energy cutoff of 400 eV for the plane wave basis set.

Free energies at 748 K and 1 bar reference pressure were computed using the harmonic approximation and the free translator/rigid rotator approximation for gas phase molecules. The accuracy of the obtained energies was further improved by performing single-point energy calculations with the ORCA program (48) on cluster models using DLPNO-CCSD(T)/cc-pVDZ (49, 50) and complete basis set extrapolated (CBS) DLPNO-MP2 calculations. The CBS extrapolation is based on the cc-pVXZ basis sets and is done separately for Hartree–Fock using three points (X = D, T, Q) and the exponential formula (51) and for the correlation part using two points (X = D, T) and the l^{-3} formula (52). More detailed information, all computed structures, corresponding total energies, and free energy corrections are provided in *SI Appendix*.

Catalytic Testing. All catalytic results were obtained using a fixed-bed quartz reactor with an internal diameter of 6 mm at 748 K and ambient pressure. The catalyst particles (200 to 280 μm) were homogeneously diluted with silicon carbide (ESK-SiC) in the range of 355 to 500 μm to ensure temperature uniformity in the catalytic bed. Catalysts were activated at 748 K for 1 h under N_2 atmosphere before the reaction. The contact time over the catalyst bed was varied via changing the catalyst loading, while the overall volumetric flow was kept constant. Each data point was measured on a fresh catalyst loading 10 min after the respective feed conditions were introduced. Internal diffusion limitation was ruled out by changing particle size and external diffusion limitation was ruled out by measuring at different total flows at similar contact times.

Methanol and water vapor at partial pressures up to 180 mbar were fed by passing N_2 through saturators which were thermo-stated by a VWR circulation thermostat at temperatures up to 333 K. Higher partial pressures were reached by addition of the respective fluid by a Shimadzu HPLC-pump combine with an aDROP direct evaporator (μSteam). DME was introduced by a Bronkhorst MFC and diluted with N_2.

The reactor effluents were transferred via a heated line into a gas chromatograph (HP 5890) equipped with an HP-PLOTQ capillary column and a flame ionization detector. The product distributions are given on a carbon basis. For the determination and quantification of CO, CO_2, and H_2 in the reaction products, we used a QMG 220 M1, PrismaPlus (Pfeiffer Vacuum) online mass spectroscopy with a continuous secondary electron multiplier (C-SEM).

Formaldehyde was quantified by condensing the reaction effluent into two bottles at 275 K for 30 min TOS with subsequent stoichiometric Hantzsch reaction as described by Nash (53) and depicted in Rxn. **6**:

[Rxn. 6]
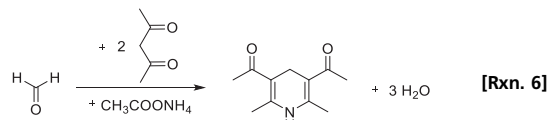
A Varian Cary 50 ultraviolet-visible spectrophotometer was used to determine the formaldehyde concentration via the absorption of the formed 3,5-diacetyl-1,4-dihydro-2,6-lutidine. In order to compare the resulting values with the yields of other products determined by GC, it was calculated an average value of formaldehyde yield for 30-min periods.

Adsorption of DME. The adsorption of DME on H-MFI(Si/Al 45) was measured in a Seteram TG-DSC 111 calorimeter connected to a high-vacuum system. About 20 mg of H-MFI zeolite was loaded in a quartz sample holder and activated at 723 K for 1 h under vacuum ($P < 10^{-4}$ mbar) with a heating rate of 5 K·min^{-1}. Afterward, the sample was cooled to 373 K and DME was introduced into the system via a dosing valve. Via carefully opening and closing the dosing valve, the pressure of DME was increased slowly in small pressure steps from $5 \cdot 10^{-3}$ to 0.4 mbar and kept at each desired pressure. The DME uptake was determined by the increase of sample weight, and the released heat was obtained by integration of the heat flux signal.

Data Availability. All study data are included in the article and/or *SI Appendix*.

1 S. L. Meisel, Gasoline from methanol in one step. *Chemtech (United States)*, **6**, 86–89 (1976).

2. C. D. Chang, Hydrocarbons from methanol. *Catal. Rev.* **25**, 1–118 (1983).

3. T. Mokrani, M. Scurrell, Gas conversion to liquid fuels and chemicals: The methanol route-catalysis and processes development. *Catal. Rev.* **51**, 1–145 (2009).

4. P. Tian, Y. Wei, M. Ye, Z. Liu, Methanol to olefins (MTO): From fundamentals to commercialization. *ACS Catal.* **5**, 1922–1938 (2015).

5. U. Olsbye *et al.*, Conversion of methanol to hydrocarbons: How zeolite cavity and pore size controls product selectivity. *Angew. Chem. Int. Ed. Engl.* **51**, 5810–5831 (2012).

6. K. Chen *et al.*, Zeolite catalysis: Water can dramatically increase or suppress alkane C–H bond activation. *ACS Catal.* **4**, 3039–3044 (2014).

7. K. De Wispelaere *et al.*, Insight into the effect of water on the methanol-to-olefins conversion in H-SAPO-34 from molecular simulations and in situ microspectroscopy. *ACS Catal.* **6**, 1991–2002 (2016).

8. J. S. Martínez-Espín *et al.*, Hydrogen transfer versus methylation: On the genesis of aromatics formation in the methanol-to-hydrocarbons reaction over H-ZSM-5. *ACS Catal.* **7**, 5773–5780 (2017).

9. J. S. Martinez-Espin *et al.*, New insights into catalyst deactivation and product distribution of zeolites in the methanol-to-hydrocarbons (MTH) reaction with methanol and dimethyl ether feeds. *Catal. Sci. Technol.* **7**, 2700–2716 (2017).

10. A. Hwang, A. Bhan, Deactivation of zeolites and zeotypes in methanol-to-hydrocarbons catalysis: Mechanisms and circumvention. *Acc. Chem. Res.* **52**, 2647–2656 (2019).

11. S. Svelle, K. Kolboe, O. Swang, U. Olsbye, Methylation of alkenes and methylbenzenes by dimethyl ether or methanol on acidic zeolites. *J. Phys. Chem. B* **109**, 12874–12878 (2005).

12. J. F. Haw, W. Song, D. M. Marcus, J. B. Nicholas, The mechanism of methanol to hydrocarbon catalysis. *Acc. Chem. Res.* **36**, 317–326 (2003).

13. S. Svelle *et al.*, Conversion of methanol into hydrocarbons over zeolite H-ZSM-5: Ethene formation is mechanistically separated from the formation of higher alkenes. *J. Am. Chem. Soc.* **128**, 14770–14771 (2006).

14. M. Bjørgen *et al.*, Conversion of methanol to hydrocarbons over zeolite H-ZSM-5: On the origin of the olefinic species. *J. Catal.* **249**, 195–207 (2007).

15. Z. Wei *et al.*, Methane formation mechanism in the initial methanol-to-olefins process catalyzed by SAPO-34. *Catal. Sci. Technol.* **6**, 5526–5533 (2016).

16. Y. Li, M. Zhang, D. Wang, F. Wei, Y. Wang, Differences in the methanol-to-olefins reaction catalyzed by SAPO-34 with dimethyl ether as reactant. *J. Catal.* **311**, 281–287 (2014).

17. T. Yashima, K. Sato, T. Hayasaka, N. Hara, Alkylation on synthetic zeolites: III. Alkylation of toluene with methanol and formaldehyde on alkali cation exchanged zeolites. *J. Catal.* **26**, 303–312 (1972).

18. Y. Liu *et al.*, Critical role of formaldehyde during methanol conversion to hydrocarbons. *Nat. Commun.* **10**, 1462 (2019).

19. A. Hwang, A. Bhan, Bifunctional strategy coupling Y2O3-catalyzed alkanal decomposition with methanol-to-olefins catalysis for enhanced lifetime. *ACS Catal.* **7**, 4417–4422 (2017).

20. A. J. Jones, E. Iglesia, Kinetic, spectroscopic, and theoretical assessment of associative and dissociative methanol dehydration routes in zeolites. *Angew. Chem. Int. Ed. Engl.* **53**, 12177–12181 (2014).

21. C. Wang *et al.*, Extra-framework aluminum-assisted initial C-C bond formation in methanol-to-olefins conversion on zeolite H-ZSM-5. *Angew. Chem. Int. Ed. Engl.* **57**, 10197–10201 (2018).

22. Y. Liu *et al.*, Formation mechanism of the first carbon–carbon bond and the first olefin in the methanol conversion into hydrocarbons. *Angew. Chem. Int. Ed. Engl.* **55**, 5723–5726 (2016).

23. A. D. Chowdhury *et al.*, Initial carbon-carbon bond formation during the early stages of the methanol-to-olefin process proven by zeolite-trapped acetate and methyl acetate. *Angew. Chem. Int. Ed. Engl.* **55**, 15840–15845 (2016).

24. M. Guisnet, L. Costa, F. R. Ribeiro, Prevention of zeolite deactivation by coking. *J. Mol. Catal. Chem.* **305**, 69–83 (2009).

25. L. Kubelková, J. Nováková, P. Jírů, "Reaction of small amounts of methanol on Hzsm-5k, Hy and modified Y zeolites" in *Studies in Surface Science and Catalysis*, P. A. Jacobs *et al.*, Eds. (Elsevier, 1984), **vol. 18**, pp. 217–224.

26. G. J. Hutchings, F. Gottschalk, R. Hunter, Comments on "kinetic model for methanol conversion to olefins" with respect to methane formation at low conversion. *Ind. Eng. Chem. Res.* **26**, 635–637 (1987).

27. N. Tajima, T. Tsuneda, F. Toyama, K. Hirao, A new mechanism for the first carbon–carbon bond formation in the MTG process: A theoretical study. *J. Am. Chem. Soc.* **120**, 8222–8229 (1998).

28. P. N. Plessow, F. Studt, Unraveling the mechanism of the initiation reaction of the methanol to olefins process using ab initio and DFT calculations. *ACS Catal.* **7**, 7987–7994 (2017).

29. J. S. Martinez-Espin *et al.*, Benzene co-reaction with methanol and dimethyl ether over zeolite and zeotype catalysts: Evidence of parallel reaction paths to toluene and diphenylmethane. *J. Catal.* **349**, 136–148 (2017).

30. S. S. Arora, A. Bhan, The critical role of methanol pressure in controlling its transfer dehydrogenation and the corresponding effect on propylene-to-ethylene ratio during methanol-to-hydrocarbons catalysis on H-ZSM-5. *J. Catal.* **356**, 300–306 (2017).

31. D. Townsend *et al.*, The roaming atom: Straying from the reaction path in formaldehyde decomposition. *Science* **306**, 1158–1161 (2004).

32. H. Schulz, M. Wei, Pools and constraints in methanol conversion to olefins and fuels on zeolite HZSM5. *Top. Catal.* **57**, 683–692 (2014).

Kirchberger et al.
Mechanistic differences between methanol and dimethyl ether in zeolite-catalyzed hydrocarbon synthesis

PNAS | 9 of 10
https://doi.org/10.1073/pnas.2103840119

CHEMISTRY

33. H. Schulz, "Coking" of zeolites during methanol conversion: Basic reactions of the MTO-, MTP- and MTG processes. *Catal. Today* **154**, 183–194 (2010).

34. S. Müller *et al.*, Hydrogen transfer pathways during zeolite catalyzed methanol conversion to hydrocarbons. *J. Am. Chem. Soc.* **138**, 15994–16003 (2016).

35. A. J. Jones, E. Iglesia, Kinetic, spectroscopic, and theoretical assessment of associative and dissociative methanol dehydration routes in zeolites. *Angew. Chem. Int. Ed. Engl.* **53**, 12177–12181 (2014).

36. S. Eckstein *et al.*, Influence of hydronium ions in zeolites on sorption. *Angew. Chem. Int. Ed. Engl.* **58**, 3450–3455 (2019).

37. C. G. Pope, Water adsorption on ZSM-5 and its aluminum free analog, silicalite. *J. Colloid Interface Sci.* **116**, 221–223 (1987).

38. G. Piccini, M. Alessio, J. Sauer, Ab initio study of methanol and ethanol adsorption on Brønsted sites in zeolite H-MFI. *Phys. Chem. Chem. Phys.* **20**, 19964–19970 (2018).

39. H. Yamazaki *et al.*, Direct production of propene from methoxy species and dimethyl ether over H-ZSM-5. *J. Phys. Chem. C* **116**, 24091–24097 (2012).

40. S. Ilias, A. Bhan, Tuning the selectivity of methanol-to-hydrocarbons conversion on H-ZSM-5 by co-processing olefin or aromatic compounds. *J. Catal.* **290**, 186–192 (2012).

41. S. Ilias, A. Bhan, Mechanism of the catalytic conversion of methanol to hydrocarbons. *ACS Catal.* **3**, 18–31 (2013).

42. L. H. Ong, M. Dömök, R. Olindo, A. C. Van Veen, J. A. Lercher, Dealumination of HZSM-5 via steam-treatment. *Microporous Mesoporous Mater.* **164**, 9–20 (2012).

43. P. N. Plessow, F. Studt, Theoretical insights into the effect of the framework on the initiation mechanism of the MTO process. *Catal. Lett.* **148**, 1246–1253 (2018).

44. J. P. Perdew, K. Burke, M. Ernzerhof, Generalized gradient approximation made simple. *Phys. Rev. Lett.* **77**, 3865–3868 (1996).

45. S. Grimme, J. Antony, S. Ehrlich, H. Krieg, A consistent and accurate ab initio parametrization of density functional dispersion correction (DFT-D) for the 94 elements H-Pu. *J. Chem. Phys.* **132**, 154104 (2010).

46. G. Kresse, J. Furthmüller, Efficient iterative schemes for ab initio total-energy calculations using a plane-wave basis set. *Phys. Rev. B Condens. Matter* **54**, 11169–11186 (1996).

47. G. Kresse, D. Joubert, From ultrasoft pseudopotentials to the projector augmented-wave method. *Phys. Rev. B* **59**, 1758–1775 (1999).

48. F. Neese, The ORCA program system. *WIREs Comput. Mol. Sci.* **2**, 73–78 (2012).

49. M. Saitow, U. Becker, C. Riplinger, E. F. Valeev, F. Neese, A new near-linear scaling, efficient and accurate, open-shell domain-based local pair natural orbital coupled cluster singles and doubles theory. *J. Chem. Phys.* **146**, 164105 (2017).

50. C. Riplinger, P. Pinski, U. Becker, E. F. Valeev, F. Neese, Sparse maps–A systematic infrastructure for reduced-scaling electronic structure methods. II. Linear scaling domain based pair natural orbital coupled cluster theory. *J. Chem. Phys.* **144**, 024109 (2016).

51. D. Feller, Application of systematic sequences of wave functions to the water dimer. *J. Chem. Phys.* **96**, 6104–6114 (1992).

52. T. Helgaker, W. Klopper, H. Koch, J. Noga, Basis-set convergence of correlated calculations on water. *J. Chem. Phys.* **106**, 9639–9646 (1997).

53. T. Nash, The colorimetric estimation of formaldehyde by means of the Hantzsch reaction. *Biochem. J.* **55**, 416–421 (1953).

Kirchberger et al.
Mechanistic differences between methanol and dimethyl ether in
zeolite-catalyzed hydrocarbon synthesis